Influenced of Ni loading on SBA-15 synthesized from oil Palm ash silica for syngas production

IOP Conf. Series: Materials Science and Engineering **702** (2019) 012024 doi:10.1088/1757-899X/702/1/012024

Influenced of Ni loading on SBA-15 synthesized from oil Palm ash silica for syngas production

H A Razak[1], N Abdullah[1], H D Setiabudi[1,2], C S Yee[1,2] and N Ainirazali[1*]

[1]Faculty of Chemical and Process Engineering Technology, College of Engineering Technology, Universiti Malaysia Pahang, 26300 Gambang, Kuantan, Pahang, Malaysia
[2]Centre of Excellence for Advance Research in Fluid Flow, Universiti Malaysia Pahang, 26300 Gambang, Kuantan, Pahang, Malaysia

*E-mail: ainirazali@ump.edu.my

Abstract. The nickel loading (1-3wt.%) effect on SBA-15 prepared via sol-gel method for dry reforming of methane (DRM) was investigated. Silica source of sodium silicate-oil palm ash (Na_2SiO_3-OPA) was obtained from extraction of OPA using mass ratio Na_2SiO_3/P123~2.9. The SBA-15 was synthesized via hydrothermal treatment reflux route at treatment temperature of 80 ^oC. A vertical stainless steel fixed-bed reactor was applied for catalytic DRM process at 800 ^oC, atmosphere pressure and ratio CH_4:CO_2 is 1:1 for 30 h. Characteristic of structure SBA-15 was successfully analyzed by TEM, indicates to the positive role of Na_2SiO_3-OPA as silica sources. XRD, BET and FTIR results revealed that 2Ni/SBA-15 exhibited high surface area (460.89 m^2/g) and pore diameter (6.53 nm), small NiO particle (14.71 nm) which assist good metal dispersion and led to better metal-support interaction. The increase of Ni loading from 1 to 3wt.% results in lowering the surface area and pore volume of catalyst as more Ni particles tend to agglomerate and positioning on the SBA-15 pores. The performance of Ni/SBA-15 catalyst in DRM decrease with the trend of 2Ni/SBA-15>3Ni/SBA-15>1Ni/SBA-15 whereby the H_2/CO followed the order of 2Ni/SBA-15≈3Ni/SBA-15>1Ni/SBA-15.These studies revealed the Ni loading influences the metal-support interaction and significantly affect the H_2/CO production.

1. Introduction

Carbon dioxide (CO_2) and methane (CH_4) are the major contributor to the greenhouse gases (GHG_S) which cause the heat entrapment in the atmosphere that led to the global warming [1]. Methane can be transformed into syngas (H_2 and CO) via three reactions which are steam reforming (SRM), dry reforming (DRM) and partial oxidation (POM). In SRM, the process was conducted in a highly endothermic reaction for considerable syngas yields that making it as a major energy consumer. Meanwhile, in POM, methane was converted into syngas with a lower H_2/CO ratio~2 with one step reaction that may affect the reaction control when high space velocities were applied [2]. Thus, DRM was gained great attention since its acknowledged as a dominant route to convert major GHG_S (CO_2 and CH_4) into syngas (H_2 and CO) compared to SRM and POM [3]. Syngas production with ratio (H_2/CO) 1.0 has been recognized in petrochemical industries as its can directly been used in production of liquid hydrocarbon via Fisher-Tropsch process [4]. Unfortunately, commercialize of DRM facing a major obstacle on the reactor blockage causes by continuous carbon formation in the system which disturbing the reaction process. Thus, researchers struggled in developing a reforming catalyst with anti-coke, anti-sintering and long life-time for better DRM process in future.

Even though noble metal based (Pd, Pt, Rh, Ru) catalysts exhibited high catalytic activity and good resistance to carbon deposition for DRM, metallic nickel (Ni) seems more attracted to the researchers due to its readily available and inexpensive compared to the noble metals [5]. Unfortunately, Ni based catalysts susceptible to fast deactivated due to the coke deposition on the active site and sintering at high temperature. Maria et al. [6] has been claimed that the selection of proper support and synthesis of method metal loading might affect the metal dispersion onto the framework that led to the high catalytic performance for DRM. It is acknowledged that ordered mesoporous materials act as a heterogenous catalyst due to its structural features as a support. On the other hand, the mesoporous materials represent high surface area and large pores that greatly contribute the dispersion of active sites and to improving mass transfer [7,8]. Among the mesoporous materials, catalysts such as MCM-41, MCM-48, MSN, Mesoporous Silica Barbara Amorphous (SBA-15) has been considered owing to their properties that contained high surface area (600-1000 m^2 g^{-1}), tunable pore dimeter (5-30 nm) and thicker pore walls (3-6 nm) [9–11]. As a matter of fact, SBA-15 possess highly ordered two-dimensional hexagonal structure with narrow pore size that be able to restrain the mobility species of metal sintering [12].

Generally, there are two common types of silica precursor that had been used for synthesis SBA-15 including tetraethyl orthosilicate ($SiC_8H_{20}O_4$, TEOS) and sodium silicate (Na_2SiO_3) [13]. Unfortunately, to prepare large amount of SBA-15 using commercial silica precursor required high cost and harmful to human kind. Thorough studies were investigated to extract silica from agricultural waste such as corn cob ash (CCA), rice husk (RH), sugarcane bagasse ash (SCBA), and oil palm ash (OPA) [14–17]. OPA was discovered as the most promising waste materials to generate high purity of silica (>60%) that normally dumped in open field without any profitable return [18]. The overall production of OPA every year was estimated around 2.6 million in Malaysia and the method of disposal normally will affect to the environment [19]. Thus, oil palm ash (OPA) waste has been used as an alternative silica sources to synthesis SBA-15 support by using reflux method.

Besides of selection suitable catalyst support, the metal loading method and the percentages of metal loading are significantly affecting the performance of the catalyst including metal particle size, metal dispersion, and metal-support interaction. Regarding of the types metal loading method, sol-gel (SG) method has been chosen due to its ability to produce uniform and homogenous dispersion with less amount of metal loading [20]. Thus, the optimum metal loading was determined to interpret the effect on the catalyst characteristic behavior and its performance. Thus, the main focus in these studies to investigate the influence of Ni loading on the SBA-15 synthesized from OPA catalysts prepared via SG methods towards DRM reaction.

2. Materials and Method

2.1 Synthesized of Na_2SiO_3-OPA

The oil palm ash (OPA) waste was supplied by Felda Lepar Hilir Palm Oil Mill, Gambang, Pahang. In order to remove unspent coarse and biomass residue, OPA was calcined in an electric furnace at 600 ^oC for 6 h. OPA was then pre-treated with 2M HCl at 80 ^oC for 3 h to eliminate the acid-soluble impurities and contaminants present. The resultant solution of HCl-OPA was filtered and washed several times with deionized water. The obtained solid residue was allowed to dry in an oven at 110 ^oC for 12 h followed by calcination at 600 ^oC for 3 h and was abbreviated as AOPA.

The reflux method was chosen to extract silica (SiO_2) from AOPA by mixing with 2.5 N NaOH under constant stirring at 120 ^oC for 3 h. The resultant suspension of sodium silicate (Na_2SiO_3) was cooled at room temperature followed by filtration and the solution obtained was assigned as Na_2SiO_3-AOPA. The amount of SiO_2 content was detected using Inductive coupled plasma-optical emission spectrometry (ICP-OES, APHA 3010) before being used for synthesis of SBA-15 support.

2.2 Catalysts preparation

The synthesis of SBA-15 was carried out using hydrothermal treatment reflux which has been declared by syahida et al. [21]. Briefly, 4.9 g of triblock poly (ethylene glycol)–block-poly (propylene glycol)–block-poly (ethylene glycol) ($EO_{20}PO_{70}EO_{20}$, Pluronic P123, molecular weight = 5800, Aldrich) was dissolved in an aqueous solution of 2M hydrochloric acid (HCl, 37 wt.%) under constant stirring at 40

^{o}C for 1 h. The Na_2SiO_3-OPA was added dropwise, pH~1 after the homogenous solution was obtained. The solution was then vigorously stirring for 24 h to form white sediment before being transferred into a hydrothermal reflux at 80 ^{o}C for 4 h. The resulting white sediment was cooled at room temperature followed by filtration, washed with D.I water, pH~7. The obtained solid product was allowed to air-dried overnight at 110 ^{o}C followed by calcination using muffle furnace at 550 ^{o}C for 3 h.

By referring the preparation technique metal loading for sol-gel method as mentioned by Xiaohua [22], an appropriate amount of Ni salt precursor, ($Ni(NO_3)_2.6H_2O$) was added slowly in SBA-15. Subsequently, 1.9 g citric acid and 1.6 mL ethylene glycol were mixed at room temperature to form a sol before being added into the suspension. The resultant green gel was then heated slowly at 80 ^{o}C until all the water fully evaporated. Thereafter, the solid residue was dried in air at 110 ^{o}C overnight followed by calcination at a heating rate of 5 ^{o}C min^{-1} up to 550 ^{o}C for 3 h. Similar procedure was repeated by varying percentages of Ni loading at 1,2, and 3 wt.% and were assigned as 1NS, 2NS, and 3NS, respectively.

2.3 Catalyst characterization

The preparation of Ni-based SBA-15 catalyst was characterized by the following technique. X-ray Fluorescence (XRF, Model S8 Tiger) was conducted to determine the chemical composition of OPA and AOPA meanwhile the amount of SiO_2 was detected using Inductively Coupled Plasma Optical Emission Spectrometry (ICP-OES, APHA 3010). Powder X-ray diffraction (XRD, Philips X' Pert MPD) was employed to analyse the crystalline phase identification, using monochromatic Cu-K$\propto$ radiation (λ) of 1.5405 $\dot{A}$ at 15 mA and 30 kV. The crystallite size (D_{NiO}) was estimated by applying the Scherrer equation:

$$D_{NiO} = \frac{0.9\lambda}{\beta \cos\theta} \quad (1)$$

where λ represents the X-ray wavelength corresponding to the Cu-K$\propto$ radiation (0.15405 nm), β is the full-width at half maximum (FWHM) and θ is the angle of diffraction corresponding to peak broadening. The specific surface area was measured by Brunauer-Emmett-Teller (BET) using AUTOSORB-1 model ASAP-2020 instrument. The pore volume (V_p) and the averages pore diameter (D_p) were obtained from Barrett-Joynet-Halenda (BJH) methods, respectively. Fourier transform infrared spectroscopy (FTIR, Nicolet Avatar 370 DTGS) was carried out using KBr compression method to determine the surface functional group of catalysts. The FTIR spectra were taken in a wavelength between range 400 to 1300 cm^{-1} with 32 scanning times. Thermogravimetric thermal analysis (PL-TGA) was employed for spent catalyst to determine the amount of carbon deposition under a mixture of air (20% O_2, 80% N_2) with heating rate 10 ^{o}C min^{-1} up to 900 ^{o}C.

2.4 Catalytic activity in the dry reforming of methane

The catalytic performance of the synthesized catalysts was performed using a vertical stainless-steel fixed bed reactor with an inner diameter of 11 mm. Approximately, 0.2 g of catalyst was loaded in the centre of reactor by quartz wool was placed at the both ends and it was subjected by H_2 reduction (H_2= 50 mL min^{-1}) at 700 ^{o}C. Then, the reaction was allowed by total flowrate 50 mL min^{-1} (STP) with feed mixture of CH_4 (99.9%) and CO_2 (99.9%) with a molar ratio 1:1 at 800 ^{o}C. The product gases were determined via Agilent Gas Chromatography (AGILENT 6890 N) which was equipped with Supelco molecular sieve 13x and Agilent Hayasep DB packed column with thermal conductivity (TCD). The following equation were used to determine the conversion of CO_2 (2), conversion of CH_4 (3), and molar ratio of H_2/CO (4):

$$CO_2\ Conversion,\ X_{CO_2}(\%) = \frac{F_{CO_2(in)} - F_{CO_2(out)}}{F_{CO_2(in)}} \times 100\% \quad (2)$$

$$CH_4\ Conversion,\ X_{CH_4}(\%) = \frac{F_{CH_4(in)} - F_{CH_4(out)}}{F_{CH_4(in)}} \times 100\% \quad (3)$$

$$Molar\ ratio\ of\ \frac{H_2}{CO} = \frac{F_{H_2}}{F_{CO}} \quad (4)$$

3. Results and Discussion

3.1 OPA and AOPA characterization

The chemical composition of OPA and AOPA was obtained using XRF analysis. The percentage of SiO_2 was the highest compared to other chemical component as observed in Figure 1. It is obviously seen that after HCl treatment, the composition of SiO_2 in OPA was increased from 47.71 % to 85.46 %. This was due to the process of acid treatment was probably related with the removal alkaline residue from the raw OPA. Based on the previous studied, Irfan Khan et al. [23] reported the amount of silica content become higher (55%) after being treated with HCl which was related with the removal of metallic impurities in the OPA material. The XRF analysis has been proven that AOPA can be as alternative low-cost material of SiO_2. Thus, the pre-treatment of OPA become significant before being extracted as Na_2SiO_3-OPA.

The optimum condition for extraction of Na_2SiO_3-OPA via hydrothermal reflux process at 100 ^oC for 3 h. Inductively Coupled Plasma Optical Emission Spectrometry (ICP-OES) analysis revealed that the amount of SiO_2 content in Na_2SiO_3-OPA was 61,021 ppm.

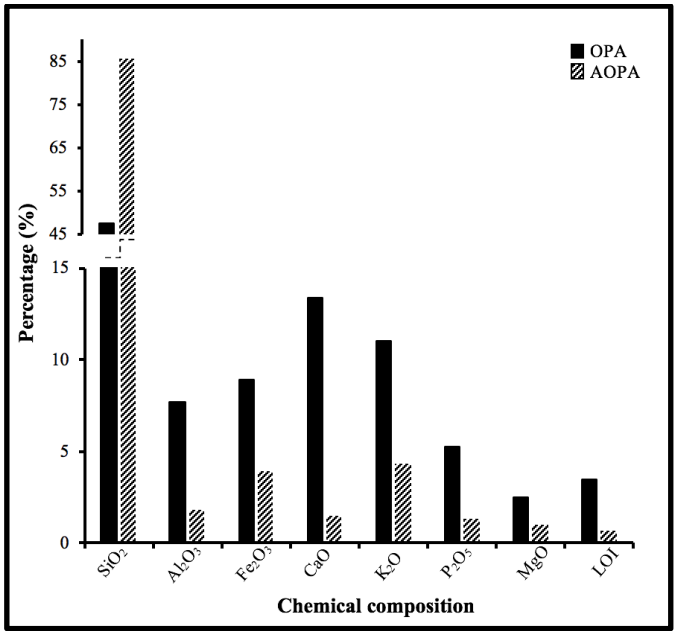

Figure 1. Percentage of chemical composition of OPA and AOPA

3.2 Characterization of catalysts

The wide-angle of XRD in the range 2θ=10^o–80^o (Figure 2) was analyzed to determine the presence of silica oxide of SBA-15 and metal crystallites of Ni supported on SBA-15 (NS). All diffractograms exhibited similar broad diffraction peak at range 2θ=15^o–35^o which centered at 22.6^o. The observed peak was assigned to the characteristics of the amorphous SiO_2 frameworks of the SBA-15 support [24]. In fact, the peak demonstrated that SBA-15 from waste OPA was successfully synthesized similar as commercial SBA-15. In addition, there are three peaks at 2θ= 38.52^o, 45.48^o, and 64.93^o were observed

for NS catalysts, corresponding to the face-centered cubic crystalline nickel oxide presence in the sample. These peaks are become more intense by increasing nickel species (1-3 wt.%) due to the stronger accessibility and incorporation between NiO particles with SBA-15 support [23]. The absence of NiO peaks for 1 wt.% Ni loading probably due to the less existence of Ni active sites that led to the undetected respective signals during the XRD measurement. Nurul et al. [25] declared that there are no peak was observed at 1Ce/SBA-15 catalyst due to the complete incorporation of 1wt.% Ce species into the SBA-15 support. Additionally, it can be obviously seen that the peaks for 2NS was broadened and less intense compared to the 3NS indicating less accumulation of NiO crystallites located onto the SBA-15 support as evidence by TEM analysis [26]. Similar occurrence was also reported by Sidik et al. [27] for Ni/MSN. They found that the peaks intensities appear for 15 wt.% was higher than 10 wt.% due to the large Ni particles that effect the aggregation of Ni species inside the support. Therefore, it can be point out that exceed of metal loading led to less dispersion of metal species due to the agglomeration of Ni crystals.

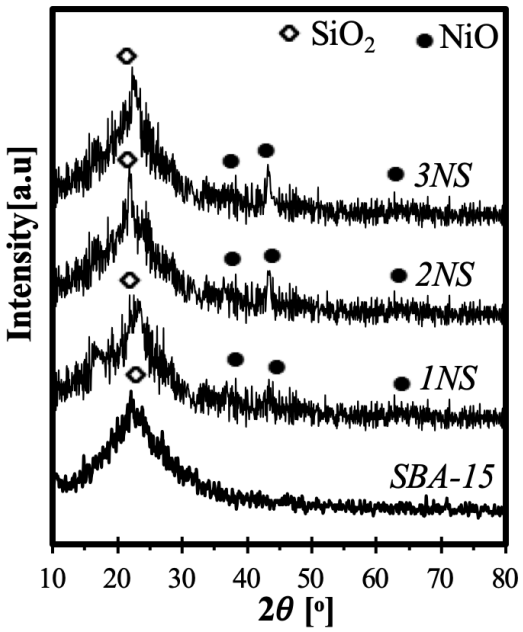

Figure 2. XRD patterns of SBA-15, 1NS, 2NS, and 3NS

The textural and physical properties of the SBA-15 and different percentages of Ni loading were displayed in Table 1. The highest BET surface area (S_{BET}) and pore diameter presented of bare SBA-15 were 524.7 m^2/g and 0.77 cm^3/g. The introduction of Ni loading (1-3 wt.%) led to the decreased of S_{BET} ranging from 490.54 m^2/g to 426.42 m^2/g due to the blockage of the pores with Ni species [28]. The change in the BET surface area was related with the different percentage of Ce species loaded into SBA-15 framework has been studied by Nurul *et al.* [29]. The results proved that the increment of Ce loading was attributed to the incorporation of Ce active sites with SBA-15 support. Additionally, it can be obviously seen the NiO crystallites sizes were 10.09, 14.71, and 16.61 nm for 1, 2, and 3 wt.% of NS that synthesized by using SG method. This result proved that SG method can generated smaller size of Ni that formed strong interaction between metal species and supports due to uniform dispersion on SBA-15 supports follows the order 2NS>3NS>1NS as evidence by XRD analysis. Previous literature by Radlik et al. [30] also was reported that NiO crystallites larger than ~12 nm easier to susceptibility of coke formation that lead to deactivation of catalyst. Apart from this, Hassani et al. [31] reported that high specific surface area was related with the reactants adsorption step which provide more active species that attributed to enhance the catalytic performance. It can be seen that, there is no significant different for the average pore volume and pore diameter which is proven that Ni species favorably dispersed outside the SBA-15 pores.

Table 1. Physical properties of SBA-15, 1NS, 2NS, and 3NS

Catalyst	Nickel content (%)	BET surface area (m^2/g)	Pore volume (cm^3/g)	Pore diameter (nm) [a]	d_{NiO} [b] (nm)
SBA-15	0	524.74	0.77	6.42	-
1NS	1	490.54	0.74	6.48	10.09
2NS	2	460.89	0.72	6.53	14.71
3NS	3	426.42	0.71	6.56	16.61

[a] Obtained from Barret-Joyner-Halenda (BJH) desorption method
[b] NiO crystallite size was calculated from XRD using Scherer equation.

According to Figure 3, TEM analysis for bare SBA-15 synthesized from OPA was conducted in order to investigate the structure and morphology of the catalyst. As it can be observed, SBA-15 (OPA) showed relatively a highly ordered hexagonal with three-dimensional network. Additionally, the apparent of hexagonal array was closely related with the formation of Si-O-Si framework influenced by appropriate amount of Na_2SiO_3-OPA and surfactant. Abdullah et al. [32] has been declared that the amount of silica to surfactant ratio was correlated with the morphology of SBA-15 framework. SBA-15 synthesized from waste OPA has been remarkable to create similar patterns as a typical feature of SBA-15 with the optimum amount of Na_2SiO_3-OPA/surfactant~ 2.9 [10, 32].

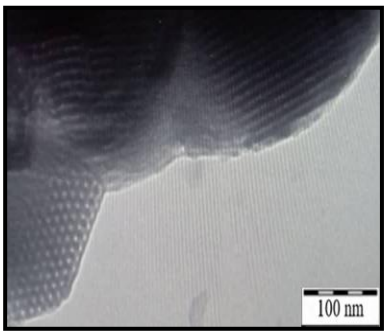

Figure 3. TEM image of SBA-15(OPA)

The distribution of 2NS on the SBA-15 support was illustrated in Figure 4. It can be clearly seen that the structure of SBA-15 was retained after insertion of 2 wt.% of Ni species. The circle dark points attributed to the Ni active sites that were well scattered onto the SBA-15 support. The well-dispersed of 2NS was corresponding with the FTIR analysis which less intense resulting good metal-support interaction of Si-O-Ni. In fact, this observation was parallel with the Ni particle size in an average (14.71 nm) as evidence by XRD analysis.

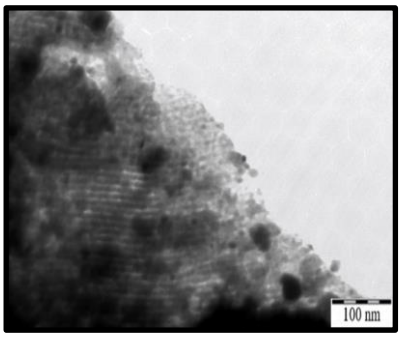

Figure 4. TEM images of 2NS with NiO particle size distribution

The functional groups present on the surface of pure SBA-15 and NS were detected via FTIR spectroscopy analysis in the range between 1300-400 cm^{-1} as shown in Figure 5. The broad absorption band at approximately 1060 and 801 cm^{-1} were corresponded to the asymmetric and symmetric of Si-O-Si stretching vibrations, respectively [5,33]. Moreover, the vibration frequency peaks at 961 and 510 cm^{-1} were attributed to the Si-O stretching vibration of Si-OH and bending vibration of framework Si-O-Si [32,34]. It can be seen that the bands observed at peak 961 cm^{-1} was reduced for all the samples after introduction of Ni into SBA-15 support. The peak of 961 cm^{-1} becomes enveloped in the band 1060 cm^{-1} probably due to the incorporation of metal ions in the silica framework, suggesting the replacement of hydrogen atoms of O-H to O-Ni to produce Si-O-Ni bond [34]. It can be observed that 2NS was less enveloped compared to the 3NS and 1NS suggesting the perfection of the incorporation Si-O-Ni. Based on the previous literature, Tomer et al. [35] revealed that the presence of Ag in SnO_2/SBA-15 was decreased the peak intensity at 961 cm^{-1} that related with the substitution of Si-O-H to form Si-O-M. Additionally, the bond observed at 1060 cm^{-1} for 3NS was weaker at the higher of Ni loading which corresponding to the partial failure of the silica network probably due to the excessive of metal ions in the Si-O-Si formation [36]. Thus, according to the results obtained, it can be concluded that the metal support interaction in the silica framework was following the order of 2NS>3NS>1NS which attribute to the appropriate amount of metal ions with strong Ni support interaction able to reduce carbon formation and prevent catalyst deactivation.

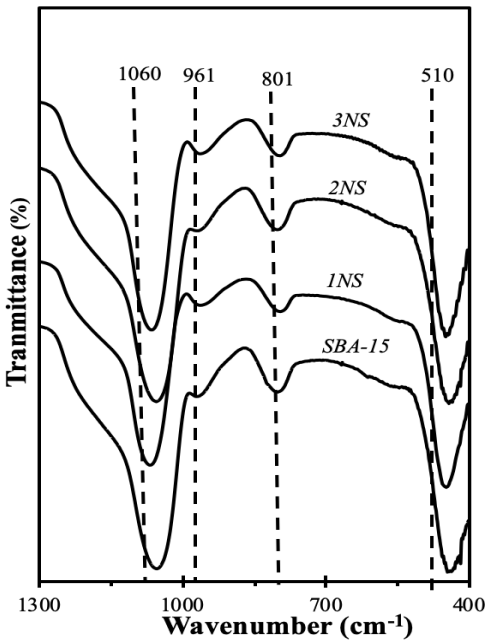

Figure 5. FTIR spectra of KBr in the range of 1300 - 400 cm^{-1} for SBA-15, 1NS, 2NS, and 3NS

3.3 Methane dry reforming reaction

The effect of different metal loading by using SG method on the catalytic performance for CH_4 conversion, CO_2 conversion and H_2/CO ratio were displayed in Figure 6. The presence of 1 wt.% of Ni loading on SBA-15 promotes the conversion of CH_4 and CO_2 which are 84.45% and 73.50%. However, the promotion was limited due to the less amount of active sites for the reaction. The performance of catalytic activity gradually increased with further increasing of Ni content 1-2 wt.%. It can be seen that 2NS exhibited the highest catalyst performance with CH_4 and CO_2 conversion of 90.26% and 93.92% due to the smaller NiO species and strong interaction as evidence by XRD, BET and FTIR. Additionally, the performance of catalytic reaction at different percentage of Ni loading synthesized by SG method followed the order of 2NS>3NS>1NS, meanwhile the average H_2/CO ratio followed the order of 2NS≈3NS>1NS. Similar observation for Ni/MgO, the catalytic performance gradually increased from the range (2-10 wt.%) yet, further increasing to 20 wt.% led to the decreased catalytic activity. This result closely related with the deposition of carbonaceous materials [37]. As suggested by Abdullah et

al. [32] the enhancement in the catalytic activity was related with Ni particles that distributed uniformly on the surface SBA-15 which related with the size of Ni species. As observed, no remarkable increase of catalytic performance with further increase in 3Ni wt.% due to the aggregation of metal species in SBA-15 support as evidence by XRD. The lowest catalytic performance for 1NS was probably due to the smallest NiO crystallite sizes that led to the Ni oxidation and accessibility of sintering. Moreover, the influence of higher percentage of Ni content on SBA-15 support is one of the vital factor that lead to carbon deposition and metal sintering has been declared by Yang et al. [38].

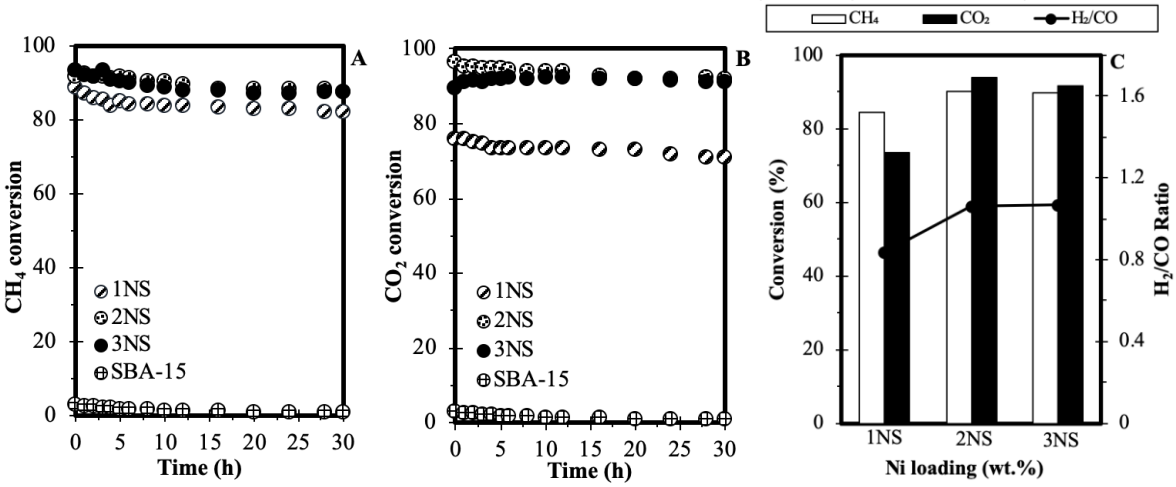

Figure 6. (A) CH_4 conversion, (B) CO_2 conversion, and (C) H_2/CO ratio of 1NS, 2NS, and 3NS. [Reaction condition m_{cat} =0.2 g, reactant flowrate = 25 mL/min, CH_4:CO_2:N_2 = 1:1:1, T=800 ^oC, P= 1 atm, t= 30 hr]

4. Conclusions

According to the present studies, a series of Ni loading with different percentage (1, 2, and 3) wt.% were loaded on SBA-15 catalyst on DRM has been investigated. The different percentage of Ni loading greatly influenced the metal distribution in the catalyst support that affect the performance of the catalytic activity. the overall characterization analyses showed that metal support interaction followed the order of 2NS>3NS>1NS, whereas the catalytic activity of catalysts followed the order of 2NS>3NS>1NS. Based on the results obtained, 2NS possessed the best catalytic activity with CH_4 and CO_2 conversion of 90.3% and 93.9% which is indicate smaller NiO particle species led to the well dispersion and strong metal support interaction as confirmation by TEM, XRD, BET, and FTIR. Thus, it can be concluded that SBA-15 synthesized from waste OPA obviously can generate similar catalytic performance as typical feature of SBA-15 with low amount of Ni loading.

Acknowledgement

The authors acknowledge the financial supports from Research Acculturation Grant Scheme Universiti Malaysia Pahang (RDU170330 & RDU1803184) and Postgraduate Grant Research Scheme (PGRS180387).

References

[1] Takahashi R, Sato S, Sodesawa T and Tomiyama S 2005 *Appl. Catal. A Gen*. **286** 142
[2] Schmal M, Brackmann R, Alves R M B and Giudici R 2019 *Int. J. Hydrogen Energy* **44** 8166
[3] Aramouni N A K, Touma J G, Tarboush B A, Zeaiter J and Ahmad M N 2018 *Renew. Sustain. Energy Rev* **82** 2570
[4] Razali S M, Asikin-mijan N and Sivasangar S 2018 *Int. J. Hydrogen Energy* **32** 186
[5] Omoregbe O, Danh H T, Nguyen-Huy C, Setiabudi H D, Abidin S Z, Truong Q D and Vo D V N 2017 *Int. J. Hydrogen Energy* **42** 11283

[6] Grzybek M, Rønning M and Da P 2018 **4** 312
[7] Karam L and El Hassan N 2018 *J. Environ. Chem. Eng.* **6** 4289
[8] Roblero J G, Pola-Albores F, Valenzuela M A, Rojas-García E, Ríos-Valdovinos E and Valverde-Aguilar G 2019 Int. J. Hydrogen Energy **42** 1854
[9] Taherian Z, Yousefpour M, Tajally M and Khoshandam B 2017 Int. J. Hydrogen Energy **42** 24811
[10] Chong C C, Abdullah N, Bukhari S N, Ainirazali N, Teh L P and Setiabudi H D 2019 *Int. J. Hydrogen Energy* **44** 20815
[11] Setiabudi H D, Chong C C, Abed S M, Teh L P and Chin S Y 2018 *J. Environ. Chem. Eng.* **6** 745
[12] Wang N, Chu W, Zhang T and Zhao X S 2012 *Int. J. Hydrogen Energy* **37** 19
[13] Wang J, Fang L, Cheng F, Duan X and Chen R 2013 *J. Nanomater* 1
[14] Okoronkwo E A, Imoisili P E, Olubayode S A and Olusunle S O O 2016 *Adv. Nanoparticles* **5** 135
[15] Vaibhav V, Vijayalakshmi U, Roopan S M 2015 S*pectrochim. Acta - Part A Mol. Biomol. Spectrosc* **139** 515
[16] Embong R, Shafiq N and Kusbiantoro A 2016 *ARPN J. Eng. Appl. Sci.* **11** 7304
[17] Razak H A, Abdullah N, Gasang J, Setiabudi H D, Yee C S and Ainirazali N 2019 *IOP Conf. Ser. Earth Environ. Sci*. **220** 012.
[18] Ismail M, Lau S K, Majid Z and Ismail M E 2009 *Asia Pacific Struct. Eng. Constr. Conf*
[19] Alsubari B, Shafigh P and Jumaat M Z J 2016 *Clean. Prod.* **137** 982
[20] Yao D, Yang H, Chen H and Williams P T 2018 *Appl. Catal. B Environ* **239** 565
[21] Bukhari S N, Chong C C, Teh L P, Vo D V N, Ainirazali N, Triwahyono S, Jalil A A, H.D. Setiabudi 2018 *Int. J. Hydrogen Energy* **1** 13
[22] Li X, Agarwal V, Liu M and Rees W S 2000 *J. Mater. Res.* **15** 2393
[23] Irfan Khan M, Azizli K, Sufian S, Man Z and Khan A S 2015 *RSC Adv*. **5** 20788
[24] Li D, Zeng L, Li X, Wang X, Ma H and Assabumrungrat S 2015 *J. Gong, Appl. Catal. B Environ.* **176** 532
[25] Ainirazali N, Ainun N, Abghazab N, Setiabudi H D and Yee S Y 2017 *J. of Science and Tech.* **10** 1
[26] Takeishi K and Akaike Y 2016 *Appl. Catal. A Gen.* **510** 20
[27] Sidik S M, Triwahyono S, Jalil A A, Aziz M A A, Fatah N A A and Teh L P 2016 *J. Chem. Eng.* **13** 71.
[28] Setiabudi H D, Lim K H, Ainirazali N and Chin S Y 2017 *J. Mater. Environ. Sci.* **8** 573
[29] Ainirazali N, Setiabudi H D and Dai-Viet N 2017 *J. Malaysian Cat.* **2** 41
[30] Radlik M, Adamowska-Teyssier M, Krztoń, K. Kozieł A, Krajewski W, Turek W and Da Costa P 2018 *Comptes Rendus Chim*. **18** 1242
[31] Hassani Rad S J, Haghighi M, Alizadeh Eslami A, Rahmani F and Rahemi N 2016 *Int. J. Hydrogen Energy* **41** 5335
[32] Abdullah N, Chong C C, Razak H A, Ainirazali N, Chin S Y and Setiabudi H D 2018 *Mater. Today Proc*. **5** 21594
[33] Chong C C, Owgi A H K, Ainirazali N, Chin S Y, Setiabudi H D 2018 *Mater. Today Proc.* **5** 21644–21651.
[34] Bukhari S N, Chin S Y, Setiabudi H D and Vo D V N 2017 *J. Environ. Chem. Eng.* **5** 3122
[35] Tomer V K, Devi S, Malik R, Nehra S P and Duhan S 2016 *Microporous Mesoporous Mater.* **219** 240
[36] Ahmed R A, Pang Y X, Olea M and Hodgson S N B 2012 **81** 71
[37] Lin L I, Lu-ming Z, Yu-hua Z and Jin-lin L I 2015 *J. Fuel Chem. Technol.* **43** 315
[38] Yang W, Liu H, Li Y, Wu H and He D 2016 *Int. J. Hydrogen Energy* **41** 1513